View metadata, citation and similar papers at core.ac.uk

brought to you by CORE

provided by Caltech Authors - Main

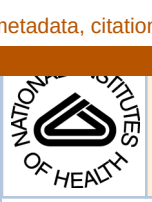

NIH Public Access

Author Manuscript

J Nucl Med. Author manuscript; available in PMC 2010 December 9.

Published in final edited form as:

J Nucl Med. 2010 February ; 51(2): 282–287. doi:10.2967/jnumed.109.065946.

Design and Optimization of Coin-Shaped Microreactor Chips for PET Radiopharmaceutical Synthesis

Arkadij M. Elizarov[1,2], **R. Michael van Dam**[2], **Young Shik Shin**[2], **Hartmuth C. Kolb**[1], **Henry C. Padgett**[1], **David Stout**[3], **Jenny Shu**[3], **Jiang Huang**[4], **Antoine Daridon**[4], and **James R. Heath**[2]

[1] Siemens Molecular Imaging, Biomarker Research, Culver City, California

[2] Nanosystems Biology Cancer Center, California Institute of Technology, Pasadena, California

[3] Department of Molecular and Medical Pharmacology, University of California, Los Angeles, California

[4] Fluidigm Corporation, South San Francisco, California

Abstract

An integrated elastomeric microfluidic device, with a footprint the size of a postage stamp, has been designed and optimized for multistep radiosynthesis of PET tracers.

Methods—The unique architecture of the device is centered around a 5-μL coin-shaped reactor, which yields reaction efficiency and speed from a combination of high reagent concentration, pressurized reactions, and rapid heat and mass transfer. Its novel features facilitate mixing, solvent exchange, and product collection. New mixing mechanisms assisted by vacuum, pressure, and chemical reactions are exploited.

Results—The architecture of the reported reactor is the first that has allowed batch-mode microfluidic devices to produce radiopharmaceuticals of sufficient quality and quantity to be validated by in vivo imaging.

Conclusion—The reactor has the potential to produce multiple human doses of ^{18}F-FDG; the most impact, however, is expected in the synthesis of PET radiopharmaceuticals that can be made only with low yields by currently available equipment.

Keywords

radiosynthesis; microfluidics; PET; ^{18}F-FDG; instrumentation

The diagnostic power of PET (1) has been demonstrated in multiple fields including oncology (2), neurology (3), cardiology (4), and inflammation (5). The advantages of PET have also been realized in drug discovery (6–8). This technique exploits biomarkers that contain positron-emitting radionuclides such as ^{18}F, ^{11}C, ^{13}N, and ^{15}O. Their short half-lives place a significant constraint on the production of these biomarkers. Unlike other chemical compounds (both drugs and contrast agents), PET probes have to be prepared hours or minutes before injection and cannot be stored. Meanwhile, it is well known that multistep chemical syntheses of many druglike compounds may take days.

For correspondence or reprints contact: Arkadij M. Elizarov, Siemens Healthcare, 6100 Bristol Pkwy., Culver City, CA 90230. arkadij.elizarov@siemens.com.

NIH-PA Author Manuscript

NIH-PA Author Manuscript

NIH-PA Author Manuscript

NIH-PA Author Manuscript

NIH-PA Author Manuscript

NIH-PA Author Manuscript

One way of overcoming this challenge is the design of synthetic routes such that the radionuclide is incorporated in the last step or close to it. Most of the known probes (such as ^{18}F-FDG (9,10) and 3′-deoxy-3′-^{18}F-fluorothymidine (11)) involve 2 synthetic steps that are precluded by radioisotope concentration and followed by purification and formulation of the injectable dose. Others (e.g., 2′-deoxy-2′-^{18}F-fluoro-5-methyl-1-β-D-arabinofuranosyluracil (12) or ^{18}F-fluoroazomycin-arabinoside (13)) require longer synthetic procedures that may limit their clinical use. The optimal radionuclide for use in PET, ^{18}F (with a half-life of 110 min), still limits the time for carrying out these processes and delivery of the product to the patient to just a few hours. On top of the short time frame, another challenge of radiosynthesis is the need for its remote manipulation because there has to be a shield between the chemist and the source of radiation.

Over the years since the introduction of PET, multiple examples of such setups have been shown ranging from user-designed systems (14) to commercially available completely automated synthesis modules (ASMs) (15). Although some of these systems demonstrate relative advantages over others, most rely on traditional chemist's tools—glass flasks or vials, heaters, and chromatography, which is designed for manipulating relatively large amounts of chemicals and volumes of solvent measured in milliliters. Meanwhile, mass of a PET tracer in a single human dose is measured in nanograms. For example, an ^{18}F-FDG patient dose measuring 740 MBq (20 mCi) contains only 300 ng of ^{18}F-FDG (assuming specific activity of 370 GBq/μmol [10 Ci/μmol]). Dissolving it in several milliliters of solvent results in a low concentration. Although low mass is beneficial for reducing the toxic effects in the patient, low concentration is generally known to reduce reaction rates and increase synthesis times.

These observations have suggested that a dramatic increase in concentrations of reagents during radiosynthesis should lead to improved effective yields, meaning more doses available for patients at the end of synthesis. The limiting reagent in these radiosyntheses is the radioisotope, and its amount cannot be increased to increase the concentration. Therefore, reducing the volume of solution is the only way to attain a high concentration of radioisotope. Volume reduction also leads to high concentrations generated with low precursor amounts. Scaling the reaction volume down from milliliters to microliters makes it impossible for the radioisotope to be handled by any of the reported ASMs without the risk of losing the entire reaction mixture. This requirement for small-volume handling has turned the attention to microfluidics.

Microfluidic devices are known for several advantages (16–18) that, if applied to the synthesis of radiopharmaceuticals, could circumvent many of the existing limitations and increase radiosynthesis output. Besides the concentration advantage, these devices promise additional benefits derived from rapid mass and heat transfer.

^{18}F-FDG (**1**) was chosen as a reference for comparing different methods because it is the most widely used PET probe whose synthesis (Scheme 1) has had the most optimization on conventional instruments. Starting with ^{18}F-fluoride, the synthesis is based on the following 3 sequential processes: concentration of the ^{18}F-fluoride from dilute ^{18}O-H_2O solution (1–10 ppm) followed by drying, ^{18}F-fluoride substitution reaction with the mannose triflate (MT) precursor (**2**) using Kryptofix2.2.2 (Sigma-Aldrich) (**3**) phase transfer reagent to allow ^{18}F-KF solubility in anhydrous MeCN, and aqueous acidic hydrolysis of the fluorinated intermediate tetraacetylated ^{18}F-fluoroglucose compound (^{18}F-FTAG) (**4**).

Traditionally, microfluidic devices rely on reactions performed in moving solutions. Several groups have applied such an approach (19,20) in radiosynthesis of PET probes (most commonly ^{18}F-FDG). Most such devices have demonstrated high yields of individual steps.

NIH-PA Author Manuscript

NIH-PA Author Manuscript

NIH-PA Author Manuscript

However, all of them relied on macroscopic batch methods for the first process (fluoride concentration, drying, and solvent exchange), and it is difficult to bridge the resulting macro–micro gap without significant material losses. Microfluidic flow-through methods for fluoride concentration are just at a conception stage (21). Also, extremely low volumes (such as 5 μL) cannot be handled by continuous-flow devices without significant sacrifice of material, meaning that the full advantage of extreme concentrations cannot be realized.

An alternative microfluidic approach relies on a batch mode of operation in all steps and requires efficiency of material transfer. This alternative approach is based on a technology termed chemical reaction circuit (CRC), which involves multilayer integrated elastomeric microfluidics (22) performing unit operations. The first such device has been produced by Lee et al. (23), who demonstrated that indeed all operations starting with ^{18}F-fluoride in ^{18}O-H_2O and yielding 2.15 MBq (58 μCi) of ^{18}F-FDG can be performed on a single chip. Although that was a major step forward in this area, it again had a micro–macro disconnect hidden in the time it would take the on-chip trap to process 2 mL of ^{18}O-H_2O (4.6 d at a reported 5 nL/s) through the on-chip column constructed using sieve valves.

Lessons learned from this work have led to the device reported here. Fundamentally different from the first CRC, the current device is designed to allow a 1,500-fold increase in throughput (up to ~3.7 GBq [100 mCi]) while ensuring seamless integration of all radiosynthesis steps that take the user from raw isotope to purified product. The key features of this chip include a relatively large (for microfluidics) coin-shaped reaction chamber and a vacuum vent (Fig. 1). The first prototype chip with these features has been described briefly in the supporting online material provided by Lee et al. (23). Although that prototype chip relied on inferior mixing processes and did not have the entire radiosynthesis integrated, it has effectively yielded the first published preclinical PET image obtained with a product of a microfluidic device. Design, analysis, and optimization of the coin-shaped reactor chips (Figs. 2 and 3) and their operation are the focus of this article.

MATERIALS AND METHODS

Materials

Solvents, acetonitrile (Riedel-deHaën), and water (Fisher Scientific) were used without further purification. MT (ABX) was used as a solution in dry MeCN (25 mg/mL), which was prepared immediately before each experiment using dry glassware flushed with N_2. Kryptofix2.2.2 solution in MeCN (50 mg/mL) was prepared weekly and stored at +4°C when not in use. A cyclotron (Eclipse HP; Siemens) was used to produce no-carrier-added ^{18}F-fluoride (specific activity, >370 GBq/μmol [10 Ci/μmol]) by 11-MeV proton bombardment of 95% ^{18}O-enriched H_2O via $^{18}O(p,n)^{18}F$ nuclear reaction.

The CRC was made from commonly used polydimethylsiloxane using pneumatic push-up valves (24). To avoid diffusion of N_2 gas from control channels into flow channels through the valve diaphragms, the control channels were filled with Krytox 100 (Dupont) fluorinated oil that did not penetrate polydimethylsiloxane, even at elevated temperatures. After initial tests, the valves were doubled to reduce their failure.

Device Fabrication

The devices were fabricated (Supplemental Fig. 1; supplemental materials are available online only at http://jnm.snmjournals.org) using the soft-lithography method (25) within a class 1,000 clean-room environment. Early CRCs were composed of 2 functional layers: a flow layer containing the coin-shaped reactor and the network of channels and a control layer that incorporated the valves and the radiator vent (placed below the reactor). A third (blank) layer was used to ensure strong bonding of the device to the substrate. Further

NIH-PA Author Manuscript

NIH-PA Author Manuscript

NIH-PA Author Manuscript

details are described in the supplemental materials. In the latest iterations, the vent was placed above the reactor, requiring an additional layer. Such 4-layer chips with 3 functional layers were fabricated at Fluidigm Corp. by a proprietary process.

Control Interface

Pneumatic operation of on-chip valves and reagent delivery was achieved by ultra-high-purity N_2 gas providing pressures of 276 MPa (40 psi) and 83 MPa (12 psi) to the control and flow manifolds, respectively. These manifolds were controlled through a BOB3 breakout controller board (Fluidigm Corp.). Control and flow lines were connected to the chip via hollow metal pins (23 gauge; New England Small Pin Corp.) and Tygon microbore tubing (Cole-Parmer East). The closing of a microvalve was driven by the activation of a channel in the manifold that pressurized the corresponding line of tubing. Banks of solenoids controlling all pressures were operated via a LabVIEW program (National Instruments).

Radiometric Analysis

The amounts of radioactive material were determined using a CRC-25R dose calibrator (Capintec, Inc.). The compositions of radioactive reaction mixtures and purified products were analyzed using thin-layer chromatography (TLC). The analyte was spotted on a silica gel–coated plate, which was subsequently developed in a 95:5 MeCN:H_2O solvent. On development, TLC plates were analyzed with an AR-2000 radio-TLC imaging scanner (Bioscan). TLC analysis of crude mixtures provided yield information, and that of purified products led to the radiochemical purity.

In Vivo Imaging

The methods related to the tumor model we used have previously been published (23). In brief, a nonmetastasizing retrovirally induced rhabdomyosarcoma was injected by intramuscular inoculation, forming tumors in 7–10 d. In these immune-competent mice, the tumors initiated a strong immune response before regression after 4–5 wk. The immune response increased metabolism that can be observed using ^{18}F-FDG PET studies.

The mouse was imaged for 15 min in a Siemens Focus 220 microPET 1 h after tail vein injection of 13.9 MBq (375 μCi) of ^{18}F-FDG, with images created at a 1.2-mm resolution using maximum a posteriori reconstruction. Immediately after the PET scan, a 10-min CT scan was acquired using a Siemens MicroCAT II small-animal CT system, using Feldkamp reconstruction to create images with a 0.4-mm resolution. PET and CT images were combined to make a fused coregistered image with AMIDE imaging software (26).

RESULTS

Ion Exchange Column and Reaction Chamber Design

The logic behind the new CRC (27) architecture was based on the requirement to process 2 mL of ^{18}O-H_2O (volume determined by cyclotron and target design) without a negative effect on CRC operation time. An off-chip column operated by on-chip valves (Fig. 3A) was considered for the radiosynthesis devices because it has a higher resin surface area per solvent volume ratio, it can be packed more efficiently (not through the chip), and it does not require sieve valves (which severely restrict the flow of solvent through on-chip columns). An optimized column had a 2-μL volume of AG1-X8 (Bio-Rad) resin bed. It trapped 99.5% of 32.4 GBq (876 mCi) of $^{18}F^-$ at a flow rate of 2 mL/min, of which 92.7% was subsequently released with approximately 5 μL of 0.5 M K_2CO_3. To simplify the design, increase the release pressure, and avoid metal contact surfaces in the ^{18}F-fluoride

NIH-PA Author Manuscript

NIH-PA Author Manuscript

NIH-PA Author Manuscript

line, chips have been later redesigned (Fig. 3B) to work with columns operated by off-chip ultra-low-volume rotary loop valves (Rheodyne).

On the basis of these results, the microreactor was in turn designed with a matching volume. A wide, flat disk shape (5-mm diameter, 255-μm height) was selected to maximize the surface area of the floor for heat transfer and temperature homogeneity and the ceiling for rapid escape of gas (Fig. 1). Short height ensures rapid thermal equilibration. The circular shape allows efficient mixing and product removal and minimizes stagnation zones in corners and pockets. Finally, such a shape provides a large circumference that can be used for many inlet and outlet ports. This shape has led to the term *coin-shaped reactor*. The architecture designed around this reactor can be seen in Figure 2 and the chip fabricated according to this design in Figure 3. All flow channels connected to the reaction chamber (except for the water channel discussed in the supplemental materials) were made 200 μm wide and 45 μm tall, with valve overlap sections 250 μm wide. Valve membranes were made 25 μm in thickness.

Serpentine Vent

The second important feature of our CRC is a serpentine-shaped multipurpose vent channel placed above the reaction chamber and separated from it by a thin, gas-permeable membrane (28). The multipurpose vent enables efficient reagent loading by providing an escape for the initial trapped gas out of the chamber while retaining the liquid. Application of vacuum in the vent allows vapor removal from the reactor and completely out of the chip while retaining the nonvolatile residues during evaporation steps. Application of pressure inside the vent during reaction steps further increases reaction rates and prevents unwanted solvent evaporation. The optimized vent comprises a serpentine pattern of 250-μm-wide 100-μm-tall channels separated from the reactor ceiling by a 50-μm gas-permeable polydimethylsiloxane membrane.

Mixing Mechanisms and Product Elution

New mixing mechanisms had to be designed because, unlike the earlier CRC, the reactions are not performed in channels in which mixing is ensured by pumping solutions through them. Five different tactics described in detail in the supplemental materials were explored to achieve mixing in the coin-shaped reactor. Although early experiments with colored solutions showed a mixing advantage in all 5 cases, the ultimate test with the actual ^{18}F-FDG radiosynthesis indicated that only the 3 methods mentioned here have led to increased product yields without negative side effects. Vacuum-assisted mixing accelerates the incoming liquid by removing all gas from the reactor before the corresponding valve is opened, resulting in instant lamination with the solution already in the reactor. The chemically assisted process relies on vigorous outgassing of CO_2 from an acid–base reaction at the interface between 2 solutions, to produce swirling. And the third process drives the mixing by pressurizing the reactor through the vent.

Efficiency or product elution is ensured by the difference in cross-sections between incoming and exit channels and positioning of these channels tangentially to the reactor circumference.

^{18}F-FDG Radiosynthesis

In summary, the coin-shaped reactor chip is designed to draw its radiosynthesis advantages over other reported devices from ultra-high reagent concentrations, pressurized reactions, loss-free material transfers, rapid temperature control, efficient mechanisms of mixing, solvent evaporation, product elution, and, most importantly, efficient integration of the complete radiosynthesis process. Sequence of chip operations, automated by controlling

NIH-PA Author Manuscript

NIH-PA Author Manuscript

NIH-PA Author Manuscript

fluid pathways using specific valves (identified by the valve number labels in Fig. 2) and pressurizing the reagents, was designed in the following manner:

- Loading and concentrating $^{18}F^-$. ^{18}F-fluoride in a dilute ^{18}O-H_2O solution (2 mL) is directed by opening valves 1 and 2 to allow flow through and trapping on ion exchange column C1. This process takes 1–2 min when driven by 69 MPa (10 psi) of N_2 gas pressure.
- Eluting $^{18}F^-$. ^{18}F-fluoride is eluted by passing 5 μL of aqueous 0.5 M K_2CO_3 solution through C1 in the direction opposite to trapping (most of the $^{18}F^-$ leaves the column without having to travel through its entire length). This solution is directed to the reactor via open valves 3, 4, and 5 using a process called dead-end filling (i.e., replacing the air inside the reaction vessel with solution having one inlet and no open outlet channels). This is accomplished by displacing the air from the reactor into the evacuated radiator vent through the thin, gas-permeable polydimethylsiloxane membrane separating the vent from the chamber.
- Drying. All valves are closed and the water is completely evaporated into the vent by heating the bottom of the reactor at 90°C while applying vacuum in the vent.
- Solubilization of $^{18}F^-$ in organic solvent. Krypto-fix2.2.2 is brought into the reactor in MeCN solution (50 mg/mL) through valve 6 by dead-end filling. With all valves closed, acetonitrile is evaporated at 65°C through the vacuum vent. Traces of water are removed as an azeotrope leaving behind ^{18}F-KF/Kryptofix2.2.2 complex (dry enough without subsequent azeotropic evaporations required in other methods), which can be redissolved in MeCN.
- Introduction of MT. MeCN solution of MT (25 mg/mL) is delivered via a single channel through valve 7. Its redissolving of ^{18}F-KF/Kryptofix2.2.2 residue is ensured by vacuum-assisted mixing.
- Fluorination. Valve 7 is closed and the reactor is heated to 75°C to drive fluorination to completion while evaporating most of the MeCN, thus super-concentrating the reaction mixture. This forms the ^{18}F-FTAG intermediate in 3 min.
- Acid hydrolysis. Three molar HCl enters the reactor through valve 8 by dead-end filling and immediately engaging in chemically assisted mixing. After the reactor is full, the valve is closed and the chip is heated at 75°C while pressure is applied in the vent to drive forward the ^{18}F-FDG–forming hydrolysis reaction by pressure-assisted mixing for 2 min.
- ^{18}F-FDG elution. ^{18}F-FDG product is eluted through valve 10 by flushing of the reactor with water entering through valve 9. Because the crude product mixture is acidic after hydrolysis, a small amount of $KHCO_3$ (3 M, 10 μL) is loaded into the water line in front of the water. It reacts with the acid and ensures that the solution is neutral for the purification step.
- ^{18}F-FDG purification. Eluted ^{18}F-FDG passes through an alumina purification cartridge (C2), which removes both Kryptofix2.2.2 and unreacted ^{18}F-F^- to generate pure ^{18}F-FDG.

Although this process has been tested, several material incompatibility issues have been discovered. Their discussion, solutions, and a modified process (Supplemental Fig. 2) are described in the supplemental material.

NIH-PA Author Manuscript

NIH-PA Author Manuscript

NIH-PA Author Manuscript

DISCUSSION

Several successful syntheses have delivered just over 100 MBq (3 mCi) of ^{18}F-FDG with yield calculated from ^{18}F-fluoride available for reaction reaching 96%. Further details and discussion are provided in the supplemental material. Higher-scale production will be possible when polydime-thylsiloxane is replaced with a suitable new material that solves the issues of ^{18}F-fluoride loss in reaction with polydimethylsiloxane and instability under aqueous basic conditions. Potentially suitable inert elastomers have been reported (29–31). The time needed to complete all necessary processes leading to ^{18}F-FDG is 14 min. The purity of the product collected after being passed through the alumina column was 99.3%.

The ^{18}F-FDG produced was considered sufficiently pure to perform small-animal PET (32). Tumor-carrying mice were injected after the doses had been diluted with saline. Further details are provided in the supplemental material. One of the small-animal PET/CT images obtained is presented in Figure 4. The tumor is clearly visible in the brachial area, confirming proper ^{18}F-FDG action. The absence of bone uptake further illustrates the chemical purity (confirming absence of ^{18}F-fluoride). Even before the optimization described in this study was completed, one of the earliest coin-shaped reactor chips had generated the first reported small-animal PET image obtained with a product of a microfluidic device (23).

To understand the advantage of the reported CRC, one can compare the results of our study with the values corresponding to modern state-of-the-art ^{18}F-FDG production in a commercial ASM such as Explora FDG$_4$ (33), which has a run time of 45 min and average decay-corrected yield of 75%. Radiochemical purity is similar (>99%). Reducing synthesis time by 30 min increases the amount of ^{18}F-based product in hand by about 20%, which can equal to several patient doses at high scale (at 20 GBq, this means an extra 4 GBq, which equals more than five ^{18}F-FDG doses). This comparison demonstrates that the effective yield is more influenced by the speed of the process than by the improvement in radiochemical reaction yield.

CONCLUSION

After repeated successful demonstrations, the coin-shaped reactor chip architecture was found suitable for robust production of multiple mouse doses of ^{18}F-FDG. The only obstacles preventing multiple human-scale dose production arise from the use of polydimethylsiloxane as a chip material. Materials allowing the chip to retain integrity during base handling and eliminating the ^{18}F loss are under development: they should enable a chip of the same fluidic design to produce multiple human doses of PET probes in a matter of minutes by coupling improved robustness and elimination of ^{18}F loss with high yields, which were demonstrated by the chip reported in this article. Such improved chips should lead to compact and flexible radiosynthesis instruments. Beyond ^{18}F-FDG, they hold more promise for the production of those PET probes that are known for their lengthy syntheses and resulting low effective yields that jeopardize the delivery of multiple patient doses. Another benefit of the new reactor will be realized in research and development of new tracers capitalizing on higher efficiencies of reaction (due to high concentrations and pressure) and shorter operation times (arising from fast reactions and solvent evaporations granted by a more than 100-fold reduction in solvent volumes). The research setting may benefit from either reusable chips with rapid cleaning cycles or disposable chips with easy exchange mechanisms. Currently, the major limitation in PET is the lack of radiopharmaceutical blockbusters. The chip technology that enables radiopharmaceutical research as described by this study should accelerate the discovery of such compounds and thus is critical for the future of PET. Finally, such reactors can have a significant impact on

NIH-PA Author Manuscript

NIH-PA Author Manuscript

NIH-PA Author Manuscript

the drug discovery process, allowing drug candidates to be labeled and studied in vivo (7,8) in a semihigh-throughput mode.

Supplementary Material

Refer to Web version on PubMed Central for supplementary material.

Acknowledgments

We acknowledge Carl Meinhart of UC Santa Barbara for theoretic investigations of on-chip processes, which will be published separately. This work was funded by Siemens Molecular Imaging, Biomarker Research, Culver City, California.

References

1. Czernin J, Phelps ME. Positron emission tomography scanning: current and future applications. Annu Rev Med 2002;53:89–112. [PubMed: 11818465]
2. Dresel, S. PET in Oncology. Berlin, Germany: Springer GmbH; 2008.
3. Mishina M. Positron emission tomography for brain research. J Nippon Med Sch 2008;75:68–76. [PubMed: 18475026]
4. Knuuti J, Bengel FM. Positron emission tomography and molecular imaging. Heart 2008;94:360–367. [PubMed: 18276820]
5. Laverman P, Bleeker-Rovers CP, Corstens FHM, Boeman OC, Oyen WJG. Development of infection and inflammation targeting compounds. Curr Radiopharm 2008;1:42–48.
6. Wang J, Maurer L. Positron emission tomography: applications in drug discovery and drug development. Curr Top Med Chem 2005;5:1053–1075. [PubMed: 16181131]
7. Boss DS, Olmos RV, Sinaasappel M, Beijnen JH, Schellens JHM. Application of PET/CT in the development of novel anticancer drugs. Oncologist 2008;13:25–38. [PubMed: 18245010]
8. Gupta N, Price PM, Aboagye EO. PET for in vivo pharmacokinetic and pharmacodynamic measurements. Eur J Cancer 2002;38:2094–2107. [PubMed: 12387835]
9. Krug B, van Zanten A, Pirson A-S, Crott R, Borght TV. Activity-based costing evaluation of [^{18}F]-fludeoxyglucose production. Eur J Nucl Med Mol Imaging 2008;35:80–88. [PubMed: 17891498]
10. Hamacher K, Coenen HH, Stocklin G. Efficient stereospecific synthesis of no-carrier-added 2-[^{18}F]-fluoro-2-deoxy-D-glucose using aminopolyether supported nucleophilic substitution. J Nucl Med 1986;27:235–238. [PubMed: 3712040]
11. Yamamoto Y, Nishiyama Y, Kimura N, et al. Comparison of ^{18}F-FLT PET and ^{18}F-FDG PET for preoperative staging in non-small cell lung cancer. Eur J Nucl Med Mol Imaging 2008;35:236–245. [PubMed: 17909790]
12. Alauddin MM, Conti PS, Fissekis JD. Synthesis of [^{18}F]-labeled 2′-deoxy-2′-fluoro-5-methyl-1-β-D-arabinofuranosyluracil ([^{18}F]-FMAU). J Label Compd Radiopharm 2002;45:583–590.
13. Grosu A-L, Souvatzoglou M, Röper B, et al. Hypoxia imaging with FAZA-PET and theoretical considerations with regard to dose painting for individualization of radiotherapy in patients with head and neck cancer. Int J Radiat Oncol Biol Phys 2007;69:541–551. [PubMed: 17869667]
14. Craciun LS, Cimpeanu C, Constantinescu O, et al. Design of an automated system for synthesis of [^{18}F]FDG for PET investigation at IFIN-HH Bucharest. Proceedings of Application of Accelerators in Research and Industry: 20th International Conference. AIP Conf Proc 2009;1:496–499.
15. Wang M, Zhang Y, Zhang Y, Yuan H. Automated synthesis of hypoxia imaging agent [^{18}F]FMISO based upon a modified Explora FDG4 module. J Radioanal Nucl Chem 2009;280:149–155.
16. Huebner A, Sharma S, Srisa-Art M, Hollfelder F, Edel JB, deMello AJ. Microdroplets: a sea of applications? Lab Chip 2008;8:1244–1254. [PubMed: 18651063]

NIH-PA Author Manuscript

NIH-PA Author Manuscript

NIH-PA Author Manuscript

17. Hashimoto M, Barany F, Soper SA. Polymerase chain reaction/ligase detection reaction/hybridization assays using flow-through microfluidic devices for the detection of low-abundant DNA point mutations. Biosens Bioelectron 2006;21:1915–1923. [PubMed: 16488597]
18. Roberge DM, Ducry L, Bieler N, Cretton P, Zimmerman B. Microreactor technology: a revolution for the fine chemical and pharmaceutical industries? Chem Eng Technol 2005;28:318–323.
19. Elizarov A. Microreactors for radiopharmaceutical synthesis. Lab Chip 2009;9:1326–1333. [PubMed: 19417895]
20. Wester HJ, Schoultz BW, Hultsch C, Henriksen G. Fast and repetitive in-capillary production of [^{18}F]FDG. Eur J Nucl Med Mol Imaging 2009;36:653–658. [PubMed: 19037638]
21. Yamahara, R.; Nakanishi, H.; Sakamoto, K.; Saiki, H.; Ozeki, E.; Iwata, R. Electrochemical micro-flow-cell for rapid and efficient concentration of [^{18}F]fluoride to aprotic solvent from [^{18}O]water [poster]. Paper presented at: Eleventh International Conference on Miniaturized Systems for Chemistry and Life Sciences (μTAS 2007); October 7–11, 2007; Paris, France.
22. Liu J, Hansen C, Quake SR. Solving the “world-to-chip” interface problem with a microfluidic matrix. Anal Chem 2003;75:4718–4723. [PubMed: 14674446]
23. Lee C-C, Sui G, Elizarov A, Tseng H-R, et al. Multistep synthesis of a radiolabeled imaging probe using integrated microfluidics. Science 2005;310:1793–1796. [PubMed: 16357255]
24. Studer V, Hang G, Pandolfi A, Oritz M, Anderson WF, Quake SR. Scaling properties of a low-actuation pressure microfluidic valve. J Appl Phys 2004;95:393–398.
25. Duffy DC, McDonald JC, Schueller OJA, Whitesides GM. Rapid Prototyping of Microfluidic Systems in Poly(dimethylsiloxane). Anal Chem 1998;70:4974–4984.
26. Loening AM, Gambhir S. AMIDE: a free software tool for multimodality medical image analysis. Mol Imaging 2003;2:131–137. [PubMed: 14649056]
27. Elizarov, AM.; Kolb, H.; Heath, J.; van Dam, RM., inventors. Siemens Medical Solutions USA, Inc, assignee. Microfluidic chip capable of synthesizing radioactively labeled molecules on a scale suitable for human imaging with positron emission tomography. International patent application. PCT/US2006/038418. Sep 29. 2006 Pub No WO 2007/041486 A2
28. Leng J, Lonetti B, Tabeling P. Microevaporators for kinetic exploration of phase diagrams. Phys Rev Lett 2006;96:084503-1–084503-4. [PubMed: 16606187]
29. Huang Y, Castrataro P, Lee C-C, Quake SR. Solvent resistant microfluidic DNA synthesizer. Lab Chip 2007;7:24–26. [PubMed: 17180201]
30. Stoyanov I, Tewes M, Koch M, Löhndorf M. Microfluidic devices with integrated active valves based on thermoplastic elastomers. Microelectron Eng 2006;83:1681–1683.
31. Song S, Lee KY. Polymers for microfluidic chips. Macromol Res 2006;14:121–128.
32. Cherry SR, Shao Y, Silverman RW, et al. MicroPET: a high resolution PET scanner for imaging small animals. IEEE Trans Nucl Sci 1997;44:1161–1166.
33. Explora FDG$_4$ [brochure]. [Accessed December 14, 2009]. Available at: http://www.medical.siemens.com/siemens/en_US/gg_nm_FBAs/files/brochures/2007/ExplorExpl4AutomatedRadiochemistry_MIND_12116493_1.pdf

NIH-PA Author Manuscript

NIH-PA Author Manuscript

NIH-PA Author Manuscript

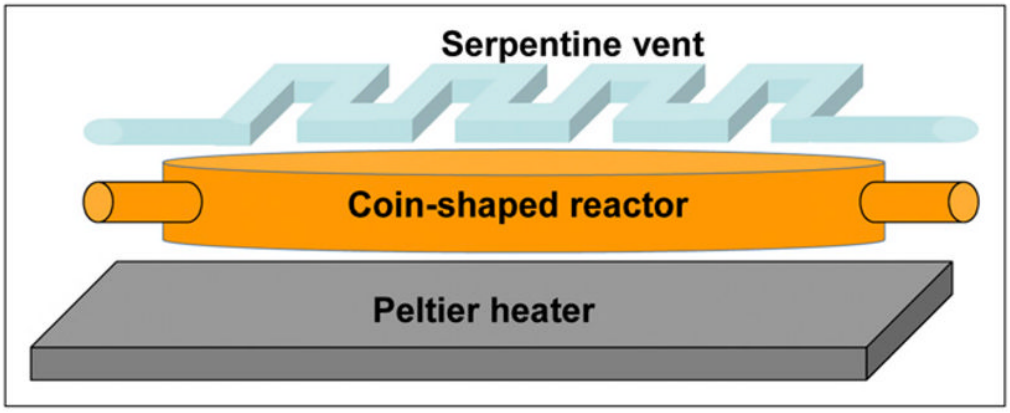

FIGURE 1.
Schematic of coin-shaped reactor designed for maximum heat and mass transfer, efficient evaporation, and convenient placement of ports.

NIH-PA Author Manuscript
NIH-PA Author Manuscript
NIH-PA Author Manuscript

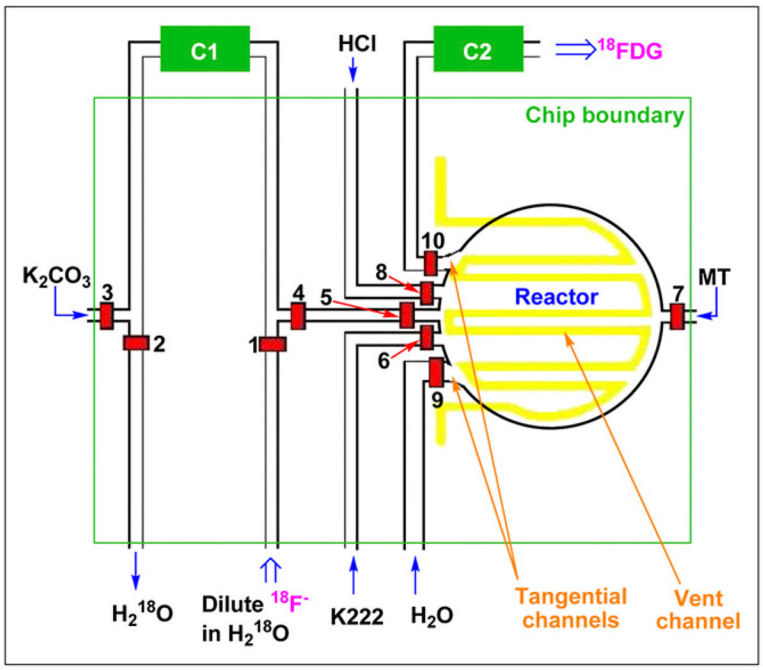

FIGURE 2.

Complete design of coin-shaped reactor chip. C1 is ion exchange column, and C2 is product purification column, both located off-chip. Reagents are introduced or removed through indicated channels, via open valves 1–10. Radiator vent is shown in yellow. Light green square outlines physical boundaries of chip. K222 = Kryptofix2.2.2.

NIH-PA Author Manuscript

NIH-PA Author Manuscript

NIH-PA Author Manuscript

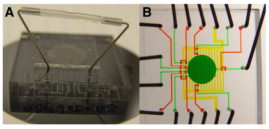

FIGURE 3.

(A) Photograph of chip with off-chip ion exchange column (C1) controlled by on-chip valves. (B) Photograph of chip designed for coupling with off-chip ion exchange column operated by off-chip loop valve. Chip is filled with dyes for visualization. Fluid network is shown in green, valves in red, and vent in yellow.

NIH-PA Author Manuscript

NIH-PA Author Manuscript

NIH-PA Author Manuscript

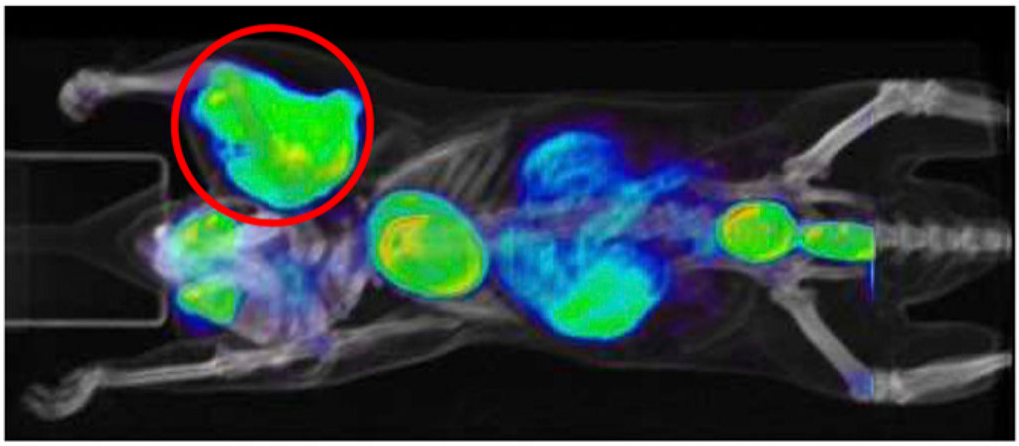

FIGURE 4.
PET image of tumor-bearing mouse.

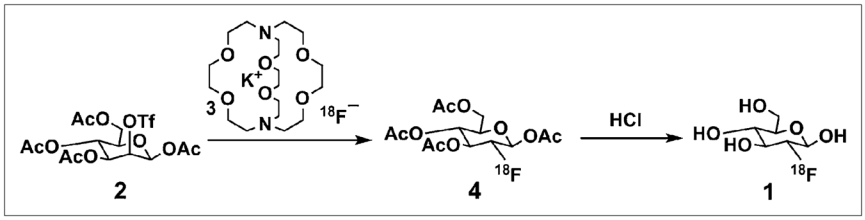

SCHEME 1.
Radiosynthesis of ^{18}F-FDG (**1**).

NIH-PA Author Manuscript
NIH-PA Author Manuscript
NIH-PA Author Manuscript